IEEE Access
Multidisciplinary | Rapid Review | Open Access Journal

Received February 14, 2017, accepted April 6, 2017, date of publication April 12, 2017, date of current version May 17, 2017.

Digital Object Identifier 10.1109/ACCESS.2017.2693300

Performances of Multitones for Ultra-Wideband Software-Defined Radar

JULIEN LE KERNEC[1], (Member, IEEE), AND OLIVIER ROMAIN[2], (Member, IEEE)
[1]School of Engineering in the Systems, Power and Energy Group, University of Glasgow, Glasgow G12 8QQ, U.K.
[2]Information Processing and System Research Lab-ETIS-UMR8051, University Cergy-Pontoise, 95000 Cergy-Pontoise, France

Corresponding author: Julien Le Kernec (julien.lekernec@glasgow.ac.uk)

ABSTRACT From the literature review, it is apparent that there is a gap in quantifying the performances of multitone waveforms specifically for radar applications and experimental results not commonly found. This paper focuses on the radar performance analysis of multitones with P3 phase-codes in simulation and experimentally to determine the effect of hardware on radar performances. For this purpose, a software-defined radar (SDR) approach has been used, including a digital core with hardware in-the-loop controlled by MATLAB and an analog front end that uses bandpass sampling and a reference channel. The proposed radar setup with processing algorithm has been evaluated in terms of processing time, showing that a real-time implementation on the latest field programmable gate array chipsets is feasible. This approach is flexible and entirely arbitrary waveforms can be generated with an instantaneous bandwidth up to 800 MHz. All the experimental results presented in Section IV are beyond the state of the art and bring novel insight into the impairment of SDR.

INDEX TERMS Chirp, OFDM, performance evaluation, quantization, ultra wideband radar.

I. INTRODUCTION

The evolution of digital technologies driven by the telecommunication industry has opened new opportunities in waveform design notably for the future 5G standard [1]–[3] for multitones with OFDM and Generalized Frequency Division Multiplexing. Even though multitones are ubiquitous in telecommunications, its adoption in operational radar is slower. The radar industry relies on proven technology and continues to use linear frequency modulated (LFM) pulses for its reliability and cost effectiveness.

Lately, the use of OFDM for the concurrent implementation of radar and communication (e.g. Radcom [4], [5]) for Intelligent Transport Systems and radar networks [6] present a challenge for conventional radar and cannot be achieved with LFM pulses. This stemmed research efforts in applying multitones to radar applications.

Another aspect of the evolution in digital technologies are the advances in converter technologies analogue to digital and digital to analogue, now enabling ultra-wideband (UWB) platforms. UWB coupled with digital cores in radar translates into submetric spatial resolution and greater flexibility in waveform design & agility. These technological advances enabled software-defined radar, which allows the simultaneous transmission of data and performing radar SAR imaging [7].

In this paper, multitones is used rather than OFDM to reflect that radar is not bound by telecommunication standards when designing waveforms and also are not necessarily orthogonal e.g. [1], [8]–[10]).

The rest of the introduction presents the state-of-the–art of multitones for radar applications in part A. Then Part B presents the problem statement stemming from Part A. Finally, part C introduces the contributions to the field from this work.

A. STATE-OF-THE-ART

Levanon's work was seminal in the development of OFDM radar and the rapid development of OFDM telecommunications drove some very significant contributions based on his book ''Radar Signals'' [11].

In [12], polyphase codes are compared to multitones in simulations. The predictable conclusion was that multitones was superior for target detection.

In [10], a generalized multicarrier waveform radar performances are evaluated through simulations against OFDM and multicarrier phase-coded waveforms showing improved

performances and Doppler resistance even if the inter-carrier interference levels are higher.

At TU Delft et al., novel signal processing capabilities for OFDM-Modulated wideband signals were proposed such as Doppler effect/scaling compensation method [13], Doppler ambiguity resolution [14], range migration compensation [15], resolving Doppler while using agility [16].

At University of Miami, a wideband multifunction software defined radar platform was developed able to perform radar, Synthetic Aperture Radar (SAR) and telecommunications using OFDM. This led to novel methods of single subcarrier phase recovery, suitable for SAR with OFDM [17], of multicarrier SAR signal processing tailored to UWB OFDM radar signals [18], of cross-range SAR reconstruction with OFDM signals using all subcarriers for phase estimation [19].

At Karlruhe Institute of Technology, RadCom, a novel OFDM joint radar-communication system - [4], [5], [28] was developed. They gave an outlook of future radar front-ends that will look like communication transceivers with multiple inputs and multiple outputs (MIMO) [29] and may use OFDM as described in [5] further demonstrated by a novel OFDM MIMO SAR concept [30]. A recent review of MIMO SAR techniques including OFDM, is available in [31] and highlights potential pitfalls with ambiguity functions.

The effort in implementing multitone waveforms for radar has produced significant contributions in software-defined radar platform development; Table 1 reports on a selection of current UWB radar platforms able to generate OFDM signals.

The underlying issue of implementation is the effect of the radio frequency equipment on radar performances. ADC converters determine the dynamic range of the radar and thus contribute greatly to detection capabilities. In order to improve power amplifier efficiency and dynamic range at converter level, Peak-to-Mean Envelope Power Ratio (PMEPR) reduction schemes are overlaid on multitones, an overview of those techniques can be found in [32].

In [33] and [34], ADC evolution prediction up to 2020 reported that wideband ADCs have not entered the saturation stage yet and research directions are mainly concentrated on increasing sampling frequencies and reducing power consumption rather than improving spectral purity or bit resolution. Furthermore, the achievable signal-to-noise ratio is not solely dependent on the effective number of bits (ENOB) but it also limited by jitter effects [35].

Oversampling can partially solve some of the hardware limitations of ADCs; but for top-shelf wideband converter such as Proteus V6 [36] equipped with the EV10AQ190 [37] or the TI ADC12J4000 [38], this solution is not feasible and too costly.

These trends pushed the emergence of a new paradigm ''Dirty RF'' [39] to compensate hardware defects digitally therefore shifting the stringent constraints on the digital core rather than the converters. Based on [33] and [34], radar applications may suffer from reduced sensitivity if the current trends are maintained. It is therefore paramount to work on digital enhancements and quantify the performances of ADC converters in order to design radar systems efficiently.

Even though there are large contributions in telecommunication to evaluate the performances of OFDM systems in simulations and experimentally driven by the market development in that sector and backed by large investments, their performances for radar are seldom found in the literature.

B. PROBLEM STATEMENT

From the literature review, it is apparent that there is a gap in quantifying the performances of multitone waveforms specifically for radar applications and experimental results are not commonly found.

This paper focuses on the radar performance analysis of multitones with P3 phase-codes (P3PC) [11] in simulation and experimentally to determine the effect of hardware on radar performances. For this purpose, a software-defined radar (SDR) approach has been used including a digital core with hardware in-the-loop controlled by Matlab and an analog front-end (AFE) that uses bandpass sampling and a reference channel. The proposed SDR setup with processing algorithm, has been evaluated in terms of processing time, showing that a real-time implementation on the latest FPGA generation [40], [41] is feasible. This approach is flexible, and entirely arbitrary waveforms can be generated with an instantaneous bandwidth up to 800MHz. All the results presented in the last section are beyond the state-of-the-art and bring novel insight into the impairment of SDR.

C. CONTRIBUTIONS

This paper builds on the results published in [42]–[45] with the experimental results from a closed-loop test and a wireless test further analyzed to get a more comprehensive view of the performances of multitones for radar applications.

This paper summarizes previously reported quantified radar performances for P3PC and LFM pulses and draws more general conclusions by extrapolating performances to general phase coding schemes for multitones. This allows gauging with quantified numbers the performances of multitones with respect to chirp on the same platform for any overlaid code. The performances for multitones are then extrapolated to different phase codes. The main difference in performance is in range, and the peak-to-mean envelope power ratio (PMEPR) will have an effect on the choice of amplifier and the input level to avoid distortions.

Extended waveform-independent metrics were used with the addition of signal-to-noise ratio, spurious-free dynamic range including and excluding harmonics were used to better understand the impact of hardware on performances. Experimental results hint towards a relationship between spurious-free dynamic range (SDFR) including and excluding harmonics with respect to time and bandwidth. Further research with different ADCs would be required to confirm this find. This information could benefit system designers in telecommunications and radar since they will be able to predict the SFDR level with harmonics from one signal measurement

TABLE 1. Main characteristics of experimental software-defined platforms from the literature.

Platform	BW (MHz)	Tested range	Sampling Scheme	Sampling frequency	Operating Frequency (GHz)	Architecture*	Supported waveforms	year
[20]	200	10m	Shannon	0.5 GS/s	77	SH/IQ	any	2014
[13]	300	N/A	Shannon	5 GS/s	10	SH/IQ	any	2010
[6]	93.1	35 m	Shannon	326.4 MS/s	6 or 24	SH/IQ	any	2010
[21]	344	20 m	Shannon	20 GS/s	2.3	DS/DD	any	2012
[22]	2000	N/A	Bandpass	5 GS/s	X-band	SH/PA/Pol	any	2013
[23]	500	N/A	Bandpass	2 GS/s	S-band	SH/PA/Pol	any	2013
[24]	800	10m	Bandpass	1.35GS/s	10-11.6	SH/FI	CW any	2007
[17]	1000	5m	Shannon	1 GS/s	7.5	SH/IQ	any	2011
[25]	50	10km	Shannon	400MS/s	S: 3.315 X: 9.6 – 10	SH/Pol	any	2009
[26]	500	55m	Shannon	1GS/s	2-18	SH/MIMO	any	2010
[27]	250	N/A	Bandpass	250 MS/s	X-band	SH/MIMO/IQ	any	2015
This work	800	60m	Bandpass	2 GS/s	10-11.6	SH	any	2017

*SH: Superheterodyne, Pol: Polarimetric, DS: direct synthesis, FI: Frequency interleaving, DD: Direct Digitization, PA: Phased Array

in the ADC. These harmonic distortions are unique to the ADCs and the signal. So by using a similar signal type like a chirp or multitone with similar coding in this case P3 codes, it is possible to predict the SFDR level from just one measurement by proportional relation between time and bandwidth with respect to the tested signal. SDR application for reduced experimental testing of performances.

A modified equation inspired from [39] is proposed to predict the maximum achievable SNR based on aperture jitter from the theoretical signal transformed from time domain to frequency domain using a fast Fourier transform (FFT). From the FFT samples in frequency domain and the jitter values from the oscillator generating the ADC clock, the maximum achievable SNR from the equation is estimated and it has been verified experimentally. Before looking at the bit resolution of an ADC, it would be important for a designer to select an oscillator based on the target SNR level.

The compression algorithm strategy reported in [42]–[45] is now feasible for real-time FPGA implementation an updated assessment of the current models against required processing power for one example of wideband receivers is presented. The benefits of this implementation are put in perspective highlighting the relaxation of reconfiguration requirements for SDR operations. This compression algorithm is conservative in computational power and is achievable using the latest FPGA chipsets based on their announced performances. It also allows flexibility in waveform generation and digitization as the algorithm needs fewer reconfigurations as one configuration deals with a range of vector sizes until the size needs to be reconfigured. It is also advantageous for ASIC implementation since it would still allow some flexibility in signal agility within the set range.

In addition, section II compared to previous publications gives a detailed account of the methodology employed to conduct this study and the lessons learnt. Section III summarizes the simulations results as well as the proposed predictive formulae, followed in section IV by the experimental results

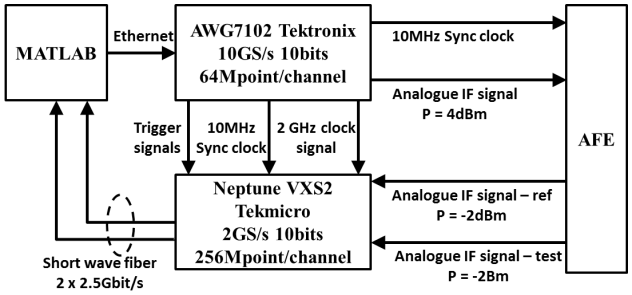

FIGURE 1. Software defined radar setup – hardware in the loop of MATLAB.

for the closed-loop and wireless test including all the metrics. The conclusions and future research directions are reported in section V.

II. METHODOLOGY

To conduct an unbiased performance evaluation of different radar signals, waveform-independent metrics must be utilized. Furthermore, to enable a direct comparison between simulations and experimental results, the processes for both should be identical. With this concept in mind, this study started with the development of the radar platform and its algorithms before anything else. This way the simulation can be modeled after the hardware that is going to be used and experimental results can be compared directly.

A. SOFTWARE-DEFINED RADAR PLATFORM

The experimental SDR setup is shown in Fig. 1 and its analogue front-end (AFE) Fig. 2 was designed to carry out experimental performance analysis of radar waveforms. Table 1 positions this work compared to the state-of-the-art and Table 2 summarizes the characteristics of the radar.

The implemented radar is particular because a reference channel is implemented for dynamic transmitter transfer

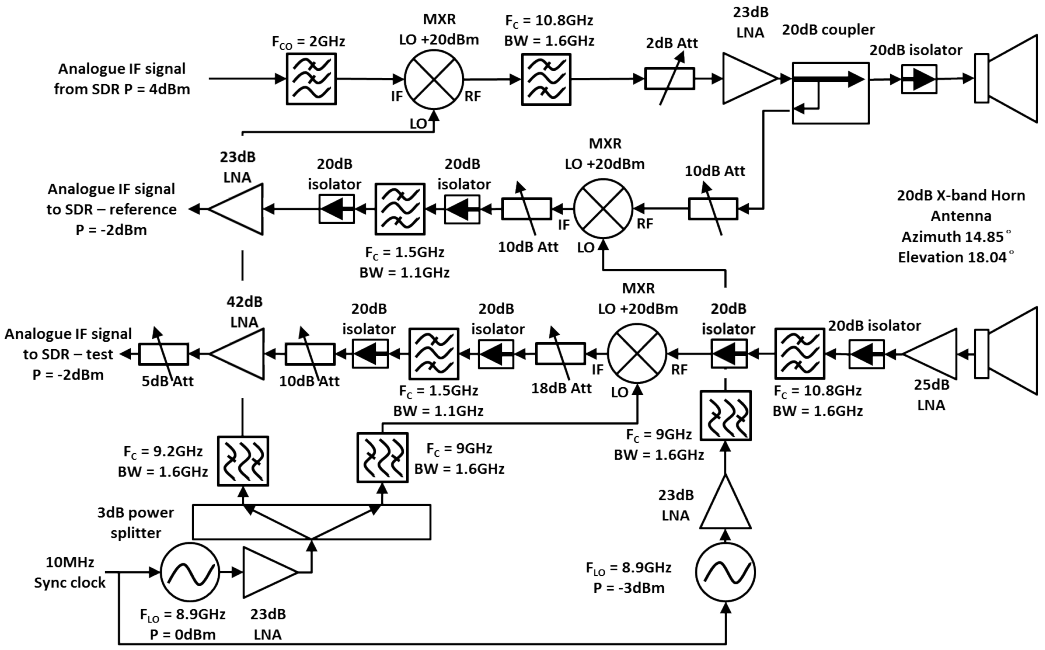

FIGURE 2. Analogue front-end.

TABLE 2. Characteristics of the experimental software-defined platform.

Intermediate frequency range (GHz)	1.1 – 1.9
Radio frequency range (GHz)	10 – 11.6
Instantaneous bandwidth (MHz)	Up to 800
Agility	1.6GHz
Antenna polarization	Vertical
Signal generator	AWG7102 [46]
• Sampling frequency (GS/s)	10
• DAC bit-resolution	10
• Analog bandwidth (GHz)	5.8
Digitizer	Neptune VXS 2 [36]
• Sampling frequency (GS/s)	2
• ADC bit-resolution	10
• Analog bandwidth (GHz)	3.3

function compensation. It is noteworthy because it is not usually implemented on operational radars which are calibrated punctually and the transfer function is considered stable for a given time which is determined empirically or arbitrarily (service time). This is accurate if considering classic radar systems with just one waveform e.g. chirp. But in the case of SDR, the waveforms are changed dynamically so that means the radar should be able to adapt dynamically as well to any changes in the transfer function and signal distortions.

The signal is directly synthesized at 10 GS/s in intermediate frequencies (IF) ranging from 1.1 to 1.9 GHz and a low pass filter removes the mirror image due to the arbitrary waveform generator DAC and its large analogue bandwidth 7.5 GHz. The IF signal feeds goes into a mixer for up-conversion in radio frequencies (RF) ranging from 10 to 10.8 GHz using a local oscillator at $F_{LO} = 8.9$ GHz which is tunable for this AFE up to 9.7GHz giving agility from 10 to 11.6GHz, and a bandpass filter removes the mirror image.

Because the maximum range available on the test ground is limited to 70m, the transmitter only needed a low noise amplifier to cover that distance. The amplifier output fed a 20 dB directional coupler that transmitted most of the energy to the transmitting antenna and fed the coupled signal to the reference channel. The receiver antenna picked up the signal returns from the scatterers feeding the test channel. The received signal is then amplified and filtered before down-conversion using the same local oscillator as for up-conversion. The signal in the reference channel is attenuated and down-converted by the same frequency $F_{LO} = 8.9$ GHz using a second oscillator which is synchronized with the other by a 10 MHz synchronization clock. In both signal paths, bandpass filters are used to limit the signal bandwidth to the 2nd Nyquist band and then amplified to avoid aliasing before digitization.

B. BANDPASS SAMPLING

The signal is bandpass [47] sampled at 2 GS/s in the second Nyquist band. Note that even though the frequencies are under-sampled, the Shannon-Nyquist law is still respected for the bandwidth digitization, thus the information is retained at the cost of energy losses (from 3 to 4.77 dB loss worst case scenario from the lowest frequency of the second Nyquist band to the highest) and an inversion of the spectrum after digitization. The advantage of using this technique was in the design of the antialiasing filter with strong rejection at the edge of the Nyquist Band and a lower relative bandwidth

TABLE 3. N[th]-order intermodulation avoidance rules for up-conversion.

Case	$F_{l1} < F_{l2} < F_{LO} < F_{H1} < F_{H2} < 2F_{LO}$	$F_{l1} < F_{l2} < F_{H1} < F_{H2} < F_{LO}$
Basics	$F_{l2} < 2F_{l1}$	$F_{l2} < 2F_{l1}$ $F_{l2} < F_{LO}/2$ & $F_{l1} < F_{LO}/4$
Validity	$n \geq 3$	$n \geq 4$
Linear	$(n-1)F_{l1} + (n-1)B < F_{LO}$	$(n-3)F_{l1} + (n-2)B < F_{LO}$
	$F_{l1\_max} = B_{max} = \frac{F_{LO}}{2(n-1)}$	$F_{l1\_max} = B_{max} = \frac{F_{LO}}{2n-5}$
Saturated	$(n-1)F_{l1} + nB < F_{LO}$	$(n+1)F_{l1} + (n+1)B < F_{LO}$
	$F_{l1\_max} = B_{max} = \frac{F_{LO}}{2(n+1)}$	$F_{l1\_max} = B_{max} = \frac{F_{LO}}{2(n+1)}$

TABLE 4. N[th]-order intermodulation avoidance rules for down-conversion.

Case	$F_{l1} < F_{l2} < F_{LO} < F_{H1} < F_{H2} < 2F_{LO}$	$F_{l1} < F_{l2} < F_{H1} < F_{H2} < F_{LO}$
Basics	X	$F_{l2} < F_{LO}/2$
Validity	$n \geq 4$ and n even	$n \geq 4$ and n even
	$F_{l2} < 2F_{l1}$	$F_{l2} < 2F_{l1}$
Validity	$n \geq 3$ and n odd	$n \geq 3$ and n odd
	$F_{l2} < 2F_{LO}/(n+1)$	$F_{l2} < 2F_{LO}/(n+3)$
$n = 3$	$B_{max} = 2F_{LO}/(n+1)$	$B_{max} = F_{LO}/2$
$n = 4$	$B_{max} = F_{L1}$	$B_{max} = F_{L1}$
$n \geq 5$	$F_{l1\_max} = B_{max} = \frac{F_{LO}}{(n+1)}$	$F_{l1\_max} = B_{max} = \frac{F_{LO}}{(n+3)}$

thus relaxing constraints on design, since it is technically impossible to obtain strong rejection near DC and this avoids having to deal with 1/f noise near DC. A 40 dB rejection in the stop bands around the second Nyquist band can be obtained – it is very difficult to design a wideband selective filter in baseband for the lower stop band towards DC that is why most filters in baseband are low pass filters not bandpass. For filters, the ratio of center frequency over the pass band should not exceed two, which translates to three eighth of the sampling frequency in the second Nyquist band (750 MHz). Two successive filters would give 60 dB rejection in the stop band. 800 MHz exceeds that condition however engineer at ''Filtek Filters'' can design such filters at the cost of 3 dB insertion loss.

C. INTERMODULATION AVOIDANCE

Concerning the up-conversion and down-conversion for UWB signals, great care has to be taken to avoid intermodulations (IM). These degrade signal purity and provoke amplitude and phase modulation.

F_{LO} Local Oscillator

$F_{l1} < F_l < F_{l2}$ IF range present at the mixer IF port

$F_{H1} < F_H < F_{H2}$ RF range present at the mixer RF port

From the perspective of maximizing the bandwidth at up-conversion, the designer should choose a local oscillator frequency greater than the RF upper bound. However, the IF input should remain in the linear operation range of non-linear devices, otherwise the n[th]-order intermodulation products are not negligible anymore. If the IF input is driven near or in saturation, it is recommended to choose a local oscillator frequency smaller than the RF range lower bound. Also in both cases, the maximum bandwidth achievable cannot exceed the IF range lower bound. In other words, the bandwidth cannot exceed an octave with respect to the IF range lower bound see Table 3 for detailed equations.

From the perspective of maximizing the bandwidth B at down-conversion, the designer should choose a local oscillator frequency greater than the RF upper bound up to third order intermodulation avoidance. For fourth-order, both schemes yield identical maximum bandwidth. And from the fifth order intermodulation avoidance, the local oscillator frequency should be smaller than the RF range lower bound, see Table 4 for detailed equations. If the bandwidth is greater than one octave and if the circuit contains any non-linear components, the designer must make sure that the second-order products do not exceed the minimum power detectable by the ADC.

The proposed AFE frequency selection ensures rejection of the intermodulation products up to the fifth for the whole bandwidth ranging from 9.5 to 12.4 GHz meaning that the agile bandwidth from 10 to 11.6 GHz is covered.

D. STUDIED WAVEFORMS

A multitude of phase codes exist to reduce peak-to-mean envelope power ratio (PMEPR better known as peak-to-average power ratio - PAPR - in communications) and an overview of the research in PMEPR reduction techniques can be found in [32]. Radar signals does not have to comply to communication standards thus allowing more flexibility in waveform design, however to enable communicating radar, a trade-off will have to be found to best fit fulfilling the radar and communication tasks.

Doppler tolerance is important in radar to avoid having to multiply Doppler filter banks in processing. To speed up implementation, P3 polyphase codes [11] were selected to reduce the PMEPR of multitones. The aim being the performance evaluation of multitones for radar applications, not the optimization of PMEPR reduction techniques. OFDM for telecommunications can have codes reaching PMEPR as high as 15 dB but commonly 10dB.

Note that multitones abide by a set of rules to avoid intermodulation interference for synthesis with DAC and acquisition with DAC, where chirp pulses can be synthesized and acquired with much higher linearity.

T is the pulse width and the orthogonal period for multitones, $B = N\delta f$ is the signal bandwidth, N is an integer and the number of tones, $\delta f = T^{-1}$ is the frequency step and $f_0 = n_0\delta f$ is the lower frequency for both signals.

Keeping the orthogonality for multitones yields the best result for impulse response. The discrete time equations of both signals chirp (1) and multitones (2) for a sampling frequency F_S and a sampling time t_S. First, a condition is set $T = Mt_S$ and M is an integer.

$$upC\,(m) = real\left(e^{j2\pi\left(n_0+N\frac{m}{2M}\right)\frac{m}{M}}\right) \tag{1}$$

$$MT\,(m) = real\left(\sum_{n=0}^{N-1} e^{j2\pi\left((n_0+n)\frac{m}{M}+\phi_n\right)}\right) \tag{2}$$

where m is the sample number with values ranging from $[0; M-1]$, $\phi_n = \frac{\pi(n-1)^2}{N}$ is the P3 phase code [11].

In order to cover various radar signal configurations from primary radar (Narrowband) to high resolution radar (UWB), various combinations of radar ambiguities and resolutions were tested with bandwidth B be set successively at 1, 10, 150 and 800 MHz, and pulse repetition periods T at 0.5, 5, 50, 500 and 1000 μs. All configurations with bandwidth-time products BT greater than 50 have been tested for both signals (see Appendix for further details).

E. WAVEFORM INDEPENDENT CRITERIA

One important metric in radar is the maximum detection range. In order to illustrate, the maximum achievable range difference (ΔR_{max}) between multitones and chirp, equation (3) is used to give the ratio of multitones over chirp.

$$\Delta R_{max} = \frac{R_{\max\_multitones}}{R_{\max\_chirp}} = 1 - \sqrt[4]{\Delta P_{avg}} \tag{3}$$

where $\Delta P_{avg} = \frac{P_{avg\_multitones}}{P_{avg\_chirp}}$ is the ratio of average transmitted power of multitones over chirp.

In order to calculate the average power, four parameters are needed the PMEPR, the power efficiency, the maximum input power at the input of the ADC within the digitization range and the peak voltage after digitization. However, to calculate the ratio, only the PMEPR and the power efficiency are needed.

1) PEAK-TO-MEAN ENVELOPE POWER RATIO (PMEPR)

To avoid distortions, a signal with high PMEPR needs to be fed to an amplifier with an input power back-off greater than what would be needed for chirp that has an ideal PMEPR of ~3 dB resulting in reduced the average output power [48], and consequently shorter maximum detection range compared to chirp. Another important aspect of PMEPR occurs at the transition between analogue and digital and vice-versa, as PMEPR increases the maximum achievable SNR decreases. The maximum achievable SNR without clipping at the ADC input is given by (4) [24].

$$SNR_{max} = P_{FS} - PMEPR - N_0 - F - B_{RX} - G \tag{4}$$

where P_{FS} is the ADC full-scale input power, N_0 is the noise density, F is the receiver noise figure, B_{RX} is the receiver bandwidth and G is the receiver gain.

2) POWER EFFICIENCY (Pe)

After digitization, the power efficiency is the ratio of in-band power after filtering over total power of the digitized signal. The in-band power is contained in the 3dB-bandwidth, here 1 MHz, 10 MHz, 150 MHz and 800MHz. The SNR/SFDR are estimated as the difference between the mean in-band power level and the noise floor/highest spurious.

3) SPURIOUS-FREE DYNAMIC RANGE

Spurious Free Dynamic Range (SFDR) including and excluding harmonics is a measure of signal purity in the frequency domain and is an important metric for high-resolution radar in the context of target recognition [49]. The IEEE standards for terminology and test methods for ADC [50] defines SFDR for a single tone but this is not adequate when working with complex signals. The SFDR is therefore estimated as the ratio between the mean value of in-band power and the highest spurious including harmonics (incl.H) (1) and excluding harmonics (excl.H) (2) inspired from IEEE standards for terminology and test methods for ADC [50].

$$\mathrm{SFDR_{incl.H}\,(dB)} = 20\log_{10}\left(\frac{\underset{f_{in\_band}}{\text{mean}}\left\{\left|X\left(f_{in\_band}\right)\right|\right\}}{\underset{f_s f_h}{\max}\left\{|X\,(f_h)|\ \text{or}\ |X\,(f_s)|\right\}}\right) \tag{5}$$

$$\mathrm{SFDR_{excl.H}\,(dB)} = 20\log_{10}\left(\frac{\underset{f_{in\_band}}{\text{mean}}\left\{\left|X\left(f_{in\_band}\right)\right|\right\}}{\underset{f_s}{\max}\left\{|X\,(f_s)|\right\}}\right) \tag{6}$$

where X is the spectrum of the ADC output determined by calculating an FFT with the maximum number of complete signal periods contained in the measured data acquisition, f_{in_band} is the input signal in-band frequency range, f_s and f_h are the frequencies of the set of harmonic and spurious spectral components.

4) SIGNAL-TO-NOISE RATIO SNR

The signal-to-noise ratio is directly linked to the maximum detectable range and detection capabilities in radar.

TABLE 5. Estimated performances for Digitizer Neptune VXS2 [36] and AWG7102 [46] based on datasheets.

Parameter	Neptune VXS2	AWG7102
ENOB	7.4 bits	N/A
Maximum SNR based on ENOB	46.3 dBFS	N/A
Aperture Jitter	[160 – 200] fs	Down to 100 fs
SNR limitation based on Jitter [51]	[54.5 – 56.4] dBFS	Up to 60.5 dBFS
Worst case bandpass sampling losses [47]	3 dB - 4.77 dB	N/A

The maximum achievable SNR for an ADC is usually expressed (6) for a single frequency.

$$\mathrm{SNR} = 6.02 \cdot \mathrm{ENOB} + 1.76 \ [dB] \tag{7}$$

where ENOB is the effective number of bits and is frequency dependent, and noise referred to here is quantization noise which unlike additive white Gaussian noise is a deterministic error and cannot be cancelled out by integration.

The maximum achievable SNR after digitization due to aperture jitter is calculated using (8) which is inspired from [39].

$$SNR_{ap} = 10 \cdot log_{10}\left(\frac{\sum_{k=0}^{K} /2S_k^2}{2\sum_{k=0}^{K} /2S_k^2\left(1 - e^{-j2(\pi f_k \sigma_j)^2}\right)}\right) - G_H \ [dB] \tag{8}$$

where K is the length of the FFT, f_k is the kth frequency at the ADC input of the bandpass sampled Nyquist band and a multiple of $\Delta \mathrm{f} = \frac{F_s}{K}$, G_H is the gain in signal power from the Hilbert transform (3 dB) ,σ_j is the standard deviation of random sampling time variations caused by the aperture jitter process, $S_k^2 = a_k^2 + b_k^2$ is the power density function (pdf) calculated in from the FFT of the Hilbert transformed baseband digitized signal. If the signal is digitized in an even Nyquist band then a spectrum inversion is necessary before the calculation of the pdf, this can be done simply in Matlab using the function 'fftshift'.

Table 5 summarizes the estimated maximum achievable SNR and the worst case scenario losses for bandpass sampling.

To extract SNR information from the measurements, equation (9) has been used to estimate SNR as follows.

$$SNR = \frac{P_{in\_band}}{N_{Rx\_BW}} \approx \frac{P_{in\_band} - G_H}{\frac{\hat{N}_{\Delta f} \cdot B_{Rx}}{\Delta \mathrm{f}}} \tag{9}$$

where P_{in_band} is the in-band power of the signal, N_{Rx_BW} is the noise power contained in the receiver (Rx) bandwidth, $\hat{N}_{\Delta f}$ is the estimated mean noise power density in a FFT bin, Δf is a frequency bin and G_H is the signal gain obtained with the Hilbert transform. The estimate for $\hat{N}_{\Delta f}$ is determined by calculating an FFT with the maximum number of complete signal periods contained in the measured data acquisition and estimating the mean noise density level between carriers and then removing the FFT gain.

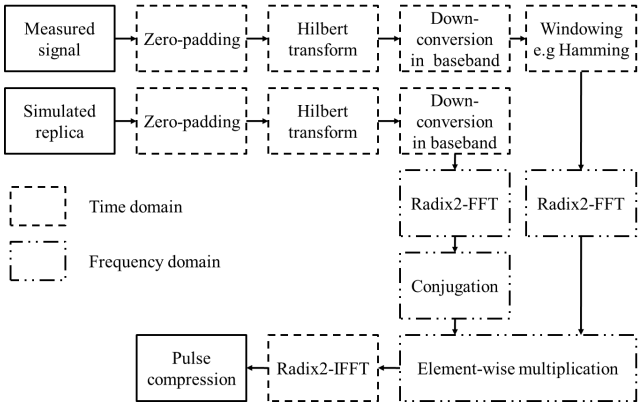

FIGURE 3. Pulse compression algorithm with radix-2 FFT.

5) PULSE COMPRESSION

In radar, the characteristics of the pulse compression are very important from the perspective of spatial resolution for the separation of two targets and peak-to-sidelobe ratio (PSLR) for contrast to avoid having a large target masking a smaller one.

In order to generate the pulse compression in range, an algorithm for matched filtering shown in Fig. 3 is proposed and is suitable for any vector size, reduces the required processing power for any vector sizes and does not suffer from edge effects.

Two input signals are necessary: the reference signal and the test signal. The reference signal is used to generate the matched filter. It can either be a digital replica or a measured replica of the generated signal. The replica can either be fixed or refreshed at a given frequency.

Since the test signal delay is unknown a priori, a sliding window that is three times the signal period is implemented for the test channel. This guarantees that whatever the signal returns delays are, a complete impulse response is generated without losses on the edges of the pulse compression. Hence, this algorithm is suitable for either the parallel or the time-interleaved architectures.

Both vectors have unit sizes equal to M (e.g. 1000) which is the signal period T (e.g. 500 ns) times the sampling frequency (2 GS/s). For faster processing, radix-2 FFT is used, thus the digitized vector length $3M$ for the test channel and M for the reference channel are zero-padded up to the next power of 2 greater than ($4M$-1). ($4M$-1) is the size of the cross-correlation between $3M$ and M. The radar system only generates the real part of the signal. The complex values of the signal must therefore be reconstructed using a Hilbert transform. The signals are digitally down-converted to baseband BB, then, a window function $w(n)$, such as Hamming, is applied over the pulse length M on the reference. The Hamming window limits the effect of inter-symbol interference (ISI) for telecommunication signals and increases the contrast of the impulse response at the cost

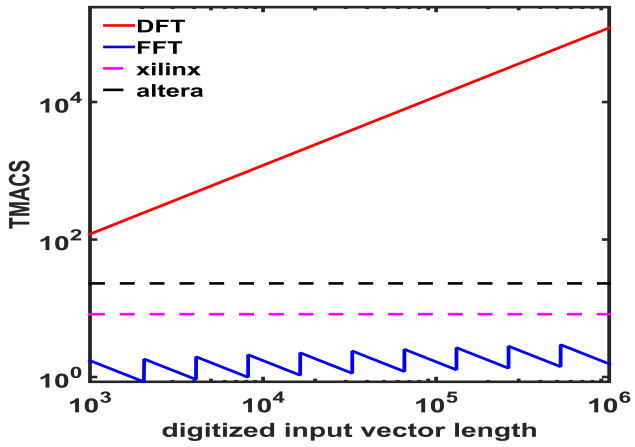

FIGURE 4. Required processing power for the proposed radar architecture in TMACS against input vector length – considering a sampling frequency of 2 GS/s, a word length of 10 bits.

of a 38 % widening of the main lobe at 3 dB. A radix-2 FFT is applied on both test and reference signals to move to frequency domain. The complex conjugate of the reference signal is multiplied element by element to the test signal. This operation is equivalent to a cross-correlation in time domain. Then, to obtain the impulse response in time domain, a radix-2 IFFT is applied. The complete pulse compression ranges from M/2 to (3M/2-1), giving a zero delayed response centered within that window. Fig.4 provides the processing power requirements in Tera Multiply Accumulate per Second (TMACS) against the vector size for a signal period comparing the requirements for the proposed algorithm as opposed to a DFT based algorithm. It can be observed from Fig. 4 that the proposed algorithm is within reach of the claimed performances of the latest FPGA chips from Xilinx (Kintex 7 UltraScale) [40] and Altera (Stratix 10) [41] using the equations from [45]. It can also be observed that for SDR flexibility is important and this algorithm only requires a reconfiguration of the FFT sizes when the vector length reaches the next power of two which would reduce the number of reconfigurations for adaptive processing with waveform agility.

F. SIMULATED PROCESSES

The simulations are basic using perfect quantization process as described in [44].

A baseline for the experimental tests was established using basic simulations. For convenience, the parameters of the simulations are given.

The signal was filtered to fit in the 2nd Nyquist band of the ADC which is 1 GHz wide between 1 and 2 GHz. Following the encoding process of the Neptune VXS II digitizer [36] and the experimental platform setup, the signal was bandpass filtered at 2GS/s in the second Nyquist band and the quantized values were floored to the nearest signed integer.

G. EXPERIMENTAL SETUP

To test the waveforms with the least distortion, a very simple experimental test bench was implemented with a

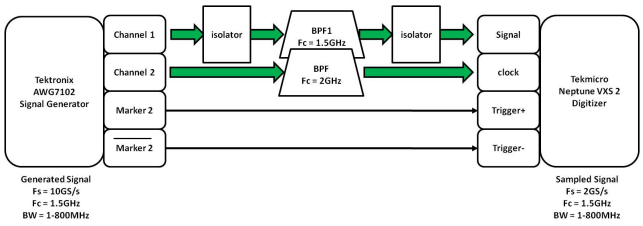

FIGURE 5. Closed-loop test set up.

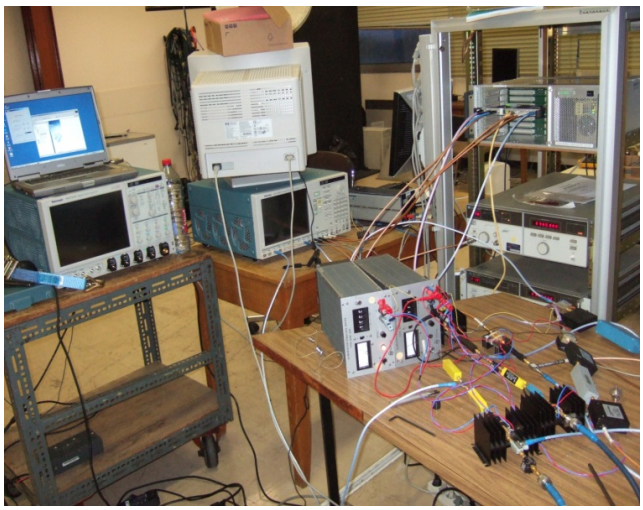

FIGURE 6. Experimental SDR platform [45].

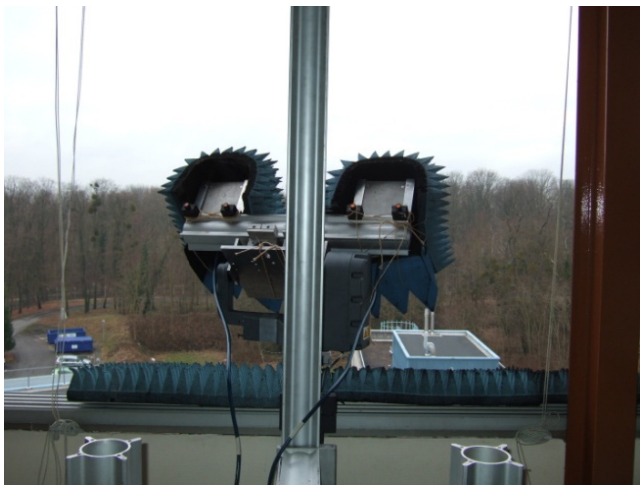

FIGURE 7. Horn antennas mounted on a tilt and pan platform pointing at the trihedral reflector [45].

DAC-isolator-filter-isolator-ADC set-up identical to the isolator-filter-isolator setup in the IF stage of either the reference or test channel presented in Fig. 2. For the closed-loop (CLL) test the input for the test channel is the measured signal and for the reference channel, is a computer generated replica. This will be followed by a wireless test as shown in Fig. 5. The wireless test on a trihedral corner reflector using the developed SDR is shown in Fig. 6 through 8.

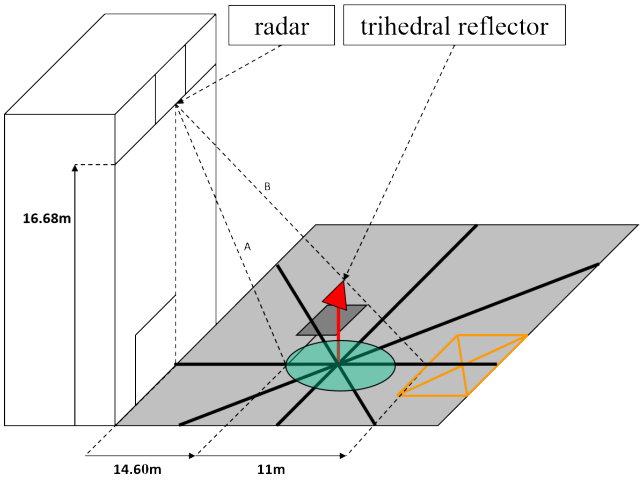

FIGURE 8. Wireless test configuration.

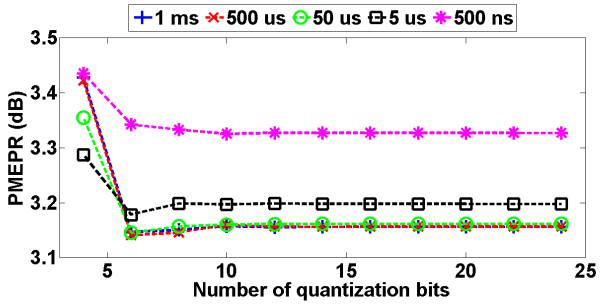

FIGURE 9. Peak-to-mean envelope power ratio of chirp with 800 MHz bandwidth with respect to number of quantization bits.

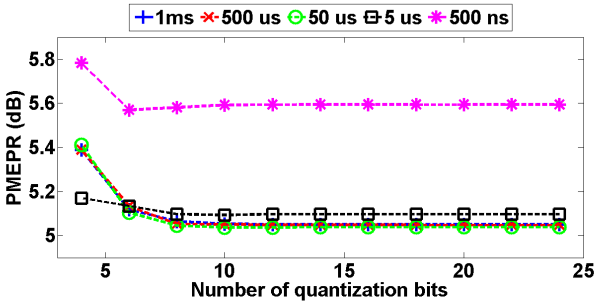

FIGURE 10. Peak-to-mean envelope power ratio of multitones with 800 MHz bandwidth with respect to number of quantization bits.

III. SIMULATION RESULTS

In this section, the simulated results for PMEPR, power efficiency, pulse compression and maximum detection range are presented. Note that the errors or differences express the variations of quantized results with respect to the performance criteria values calculated using 64-bit floating point precision.

A. PEAK-TO-MEAN ENVELOPE POWER RATIO (PMEPR)

The PMEPR of chirp (Fig. 9) varied between 3.01 dB and 3.54 dB for large BT products due to filtering effects. The PMEPR for multitones (Fig. 10) was in the range

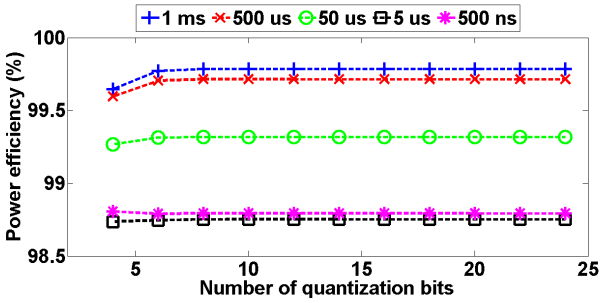

FIGURE 11. Power efficiency of chirp with 800 MHz bandwidth with respect to quantization.

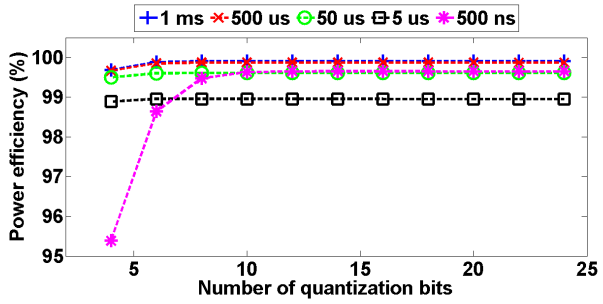

FIGURE 12. Power efficiency of multitones with 800 MHz bandwidth with respect to quantization.

5.03 dB to 5.63 dB which matched the expected PMEPR reduction for P3 phase codes [11] taking into account the signals are centered on 1.5GHz and are not in baseband. At 10-bit of resolution, the PMEPR difference of chirp compared to multitones varied between 1.65 and 2.6 dB between multitones and chirp. The simulation results showed that PMEPR varied at most by 0.4 dB from 4 to 10 bits and is stable up to 24bits. Quantization effects can therefore be neglected with respect to PMEPR.

B. POWER EFFICIENCY (Pe)

As the bandwidth-time product increases, so does the power efficiency as was expected since the Nyquist band was fixed. Indeed, if the signal bandwidth increases with respect to a fixed noise bandwidth set by the Nyquist bandwidth then it makes sense that the spectral efficiency increases with an increasing bandwidth. Also an increased signal period results in a higher FFT gain then again increasing the SNR. The relative error on power efficiencies between both chirp and multitones decreased as the BT product increased. Multitones (Fig. 11) have higher power efficiency than chirp (Fig. 12); the error was lower than 4 %. Both waveforms were equivalent and a minimum resolution of 6 bits is required have an error lower than 2% of the ideal power efficiencies for any of the studied BT products and signals.

C. MAXIMUM DETECTION RANGE

The maximum detection range (3) is calculated as a function of the average power computed as a function of PMEPR

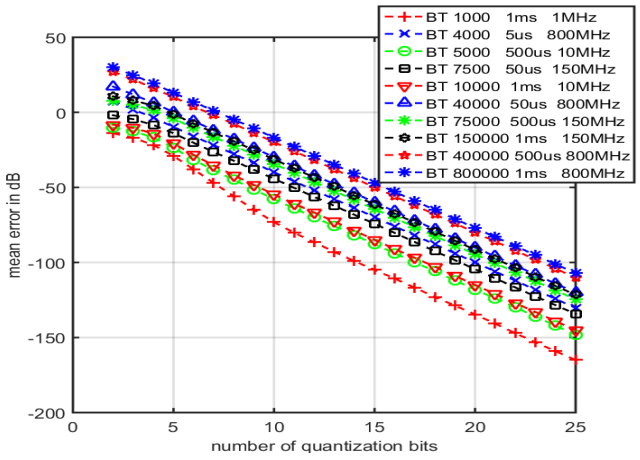

FIGURE 13. Mean error on pulse compression with respect to the number of quantization bits for multitones.

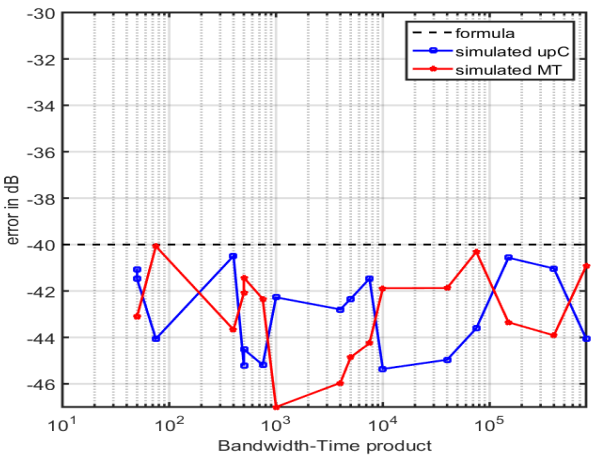

FIGURE 14. Mean error on pulse compression using predictive formula (10) compared to the set threshold with respect to BT product.

and power efficiency. The difference at 10-bit resolution is between 1.65 to 2.6 dB; therefore, the maximum detection range of chirp is 10 % to 15 % larger than for multitones.

If an application is constrained in power consumption, chirp is a better option especially at lower resolutions; indeed, its lower PMEPR makes it more efficient for amplifier stages and for AD/DA conversion.

The fact that differences between the signals were getting closer as the bandwidth was increasing is worthy of notice. Since a constant wideband receiver bandwidth of 1 GHz is assumed for any BT products, the results in operational radar would more closely match the wideband results. In practice, the signal bandwidth and the receiver bandwidth would be closely match to maximize SNR and filter out of band unwanted signals. In that case, it would be fairer to assume a 10 % difference in detection range.

D. PULSE COMPRESSION

The quantization process does not affect the main characteristics of the pulse compression (main lobe widths at 3, 6, 10 dB, 1st order sidelobe levels and distances). The maximum errors encountered are of the order of 2 times the sample speck. Indeed, the time sampling affects the time/distance resolution and causes errors in the pulse compression when the distances measured are of the order of the sample speck (equal to the speed of light divided by twice the IF sampling frequency. To illustrate, the sample speck at 2 GS/s is 7.5 cm, so when measuring distances for a signal of 800 MHz bandwidth, the main-lobe width should theoretically be 18.75 cm but the simulated main-lobe width is 33.75 cm which is caused by the time resolution of the quantized signal. When comparing the simulated pulse compressions with 4 to 24 bits against the ideal compression with 64 bits floating point, the differences between both chirp and multitones are negligible.

Quantization has no effect on the characteristics of main-lobe and side lobes for either signals. Chirp has better contrast overall with consistently about 2 dB more than multitones.

The mean error against the number of bits is shown in Fig. 13 for multitones.

For a perfectly linear digitizer as assumed in the model ENOB is equal to the number of resolution bits. An empirical analysis of the mean error on pulse compression led to the following: for a mean error of -40 dB or lower on amplitude and phase across the entire pulse response is obtained for a minimum resolution given in (10) and its results are shown in Fig. 14-15.

$$\text{minimum resolution} = \lceil 2log_{10}(BT) \rceil + \lfloor PMEPR_{lin} \rfloor \quad (10)$$

where BT is the bandwidth-time product of the signal, and $\text{PMEPR}_{\text{lin}}$ is the linear peak-to-mean power ratio of the signal.

For a BT product of 40000 a chirp with PMEPR = 3.01 dB and multitones with PMEPR $\approx$ 5.5 dB, the minimum required resolutions were respectively 12 bits and 13 bits. This means that for the same degree of accuracy multitones require one extra bit of resolution for phase coding schemes equivalent to P3 phase codes and more for codes with higher PMEPR.

Another way to look at predicting it from a theoretical and practical standpoint, is from the front-end design perspective. The receiver chain of a radar system is set so that the noise level is of the order of the two least significant bits of ADC. This avoids deterministic errors on signal quantization that would cancel the benefit of integration to improve SNR.

The derived resolution is the minimum required to obtain a desired SNR without integration without white noise in the digitizer. However, a rule of thumb in radar is to tune the gain of the receiver chain in order to have white noise covering the two lower significant bits of the digitizer. This would randomize the process and thus allow integration. Depending on the application and considerations for dwell time and other system requirements integration capabilities might be limited.

The maximum contrast with the signal at full scale for a single pulse compression is approximated by (12).

$$\begin{aligned} C_{max} &\approx 10log_{10}(G_{FFT}) - 10log_{10}(SNR_{max}) \\ &\leq 20log_{10}(BT) \end{aligned} \quad (11)$$

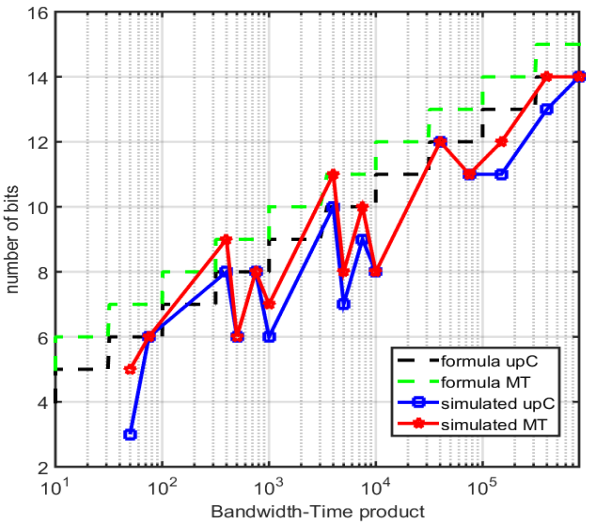

FIGURE 15. Simulated number of bits to obtain a mean pedestal error at −40 dB or lower against predictive formula (10) with respect to BT product.

where SNR_{max} is defined in equation (5). We have discussed the link between SNR_{max} and the resolution of the digitizer and the rule of thumb used in the radar community to avoid deterministic noise. SNR_{max} in (5) can be expressed as a function of the number of bits as shown in (12):

$$SNR_{max} \approx 20log_{10}\left(2^{(N-2)}\right)+G_{OS}-PMEPR-Loss \equiv N \approx \left\lceil log_2\left(10^{\frac{\mathrm{SNR}_{max}+PMEPR+Loss-G_{OS}}{20}}\right)+2\right\rceil \quad (12)$$

where G_{OS} is the gain obtained when oversampling the signal.

The proposed equations 10 and 12 can be used to gauge digitizer resolution requirements depending on application parameters for a single pulse compression. They still need to be proved experimentally but this is beyond the scope of this article.

E. SYNTHESIS

From the simulations results, it can be concluded that provided with 10-bit resolution using the DAC AWG7102 [46] and ADC Netptune VXS 2 [36]) are sufficient in terms of reaching near ideal values for PMEPR and power efficiencies. With advances in DAC from Tektronix [46] and ADC from Tekmicro [36], it is now possible to generate signals in IF directly in X band and acquire signals in S band with 10-bit resolution and as high as 70GHz with DPO70000SX [46] with 8-bit resolution.

It has been shown empirically that magnitude and phase errors in pulse compression were BT-product dependent. From (10), it can be observed that the number of bits required to reach the same error were dependent on PMEPR. So higher PMEPR using typical telecommunication coding schemes will yield higher constraints on ADC resolutions for the same error requirement on compression. These extra bits will come at the expense of power consumption if it is possible or reduced sampling frequency by splitting the receiver bandwidth between several ADCs.

TABLE 6. Relative error between measurements and simulations, and relative error between measured chirp and multitones (MT) for the closed-loop test and the wireless test (WT) for both the reference channel (RC) and the test channel (TC).

	CLL	WT - RC	WT - TC
chirp (dB)	[3;4.1]	[3.2;5.2]	[3.3;6.2]
multitones (dB)	[5;6]	[3.7; 4.26]	[4.2;5.7]
MT-chirp (dB)	[1.2;2.6]	[-0.9;1]	[-0.35;0.9]
chirp: (meas –sim) (dB)	[0.1;0.95]	[0.2-2.2]	[0.35;3.1]
MT: (meas –sim) (dB)	[0;0.85]	[-1.85;-1.3]	[-1.4;0.4]

IV. EXPERIMENTAL RESULTS

This section reports on the measurements for both the closed-loop (CLL) test and the wireless test (WT) as described in section II part A and G and compares them to the simulation results.

A. PEAK-TO-MEAN ENVELOPE POWER RATIO

For the closed-loop test, the measured values of PMEPR for multitones and chirp were consistent with simulations with a difference under 1 dB. The PMEPR for multitones was in the range of 5 dB to 6 dB. The differences in PMEPR between both waveforms are within the range 1.2 dB to 2.6dB.

For the wireless test, the PMEPR values varied from simulations with a difference between measured and simulated values of up to 2.2dB and 3.1dB respectively on the reference and test channel. The PMEPR for multitones was on average 1.5dB lower than expected. The differences in PMEPR between both waveforms are within the range ±1dB.

In both cases, the gap between the waveforms was reduced when the signal bandwidth was equivalent to the receiver bandwidth and increasing the resolution from 8 to 10 bits had negligible effect on PMEPR with about 0.1 dB of difference.

The anti-aliasing filter bandwidth was between 0.95 and 2.05 GHz which was wider than the 2nd Nyquist band. Some energy from the neighboring Nyquist bands may have folded into the Nyquist band of interest, thus the recorded signals could be distorted. Furthermore, the bandwidth gain was not constant over the entire band. These factors may have degraded the PMEPR. However, the simulated and measured results on PMEPR match for the closed-loop, however the full setup test seems to favor multitones as chirp presented stronger degradation. Although it is to be noted that in the test channel although there is only one strong reflector in the scene, the signal is a composite of all the returns from the environment.

Table 6 summarizes the measured results.

B. POWER EFFICIENCY

The power efficiency was within 15-25% of the expected value for narrow bandwidth (1/10 MHz) and/or low BT products (<1000) and within 3% for larger bandwidth (150/800 MHz) and/or larger BT (>10000) and its general behavior was consistent with simulations as shown

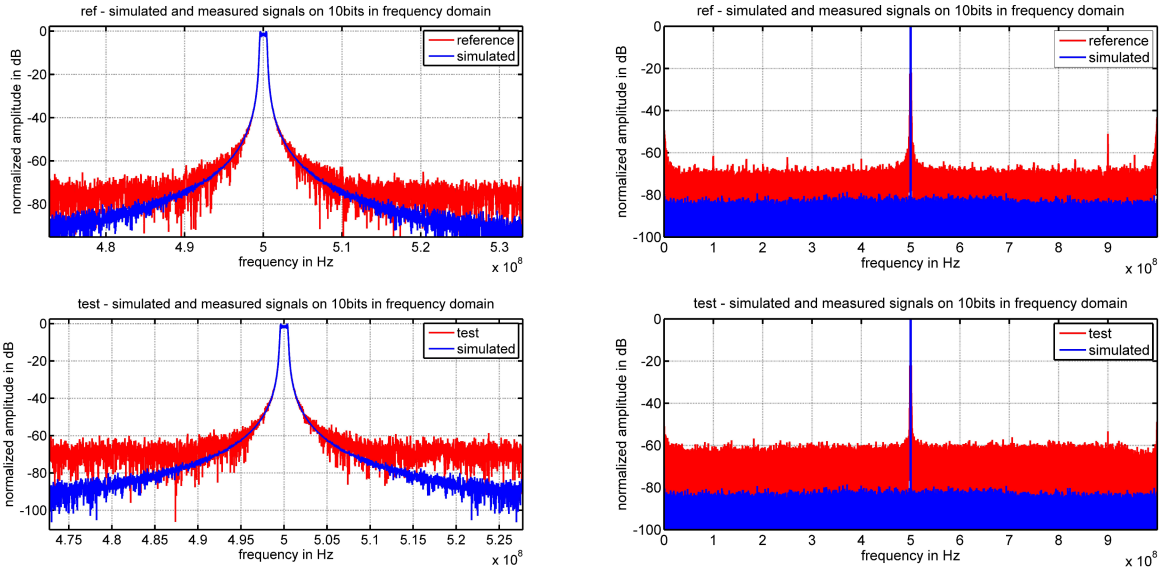

FIGURE 16. Measured spectra with 1 MHz bandwidth (left) chirp (right) multitones (top) reference channel (bottom) test channel a 10-bit resolution.

TABLE 7. Relative error between measurements and simulations, and relative error between measured chirp and multitones.

setup	bandwidth	1 MHz	10 MHz	150 MHz	800 MHz
CLL	ε_{SIM}	<15 %	<7 %	<7 %	<5 %
	ε_{MT}	<3.8%	<6.5 %	<5.7%	<2 %
WT-RC	ε_{SIM}	<12%	<5%	<12%	<1%
	ε_{MT}	<0.01%	<0.06%	<0.02%	<0.02%
WT-TC	ε_{SIM}	<24%	<10%	<11%	<2%
	ε_{MT}	<0.025%	<0.015%	<0.01%	<0.015%

in Table VII. Also, the difference between 8 and 10 bit resolutions was at most 1 %, compared to 2 % in simulation and hence had negligible impact as expected. The difference in values compared to simulations is mostly due to signal distortions caused by hardware. Also the relative error mean value of spectrum efficiency between chirp and multitones is about 2% on average in closed-loop and negligible in open loop as shown in Table VII.

Fig. 16-17 display the measured spectrum of chirp and multitones for 1 and 800 MHz for a period of 50μs. Fig. 17 illustrates the unevenness of the gain response. Some unwanted signals and stronger noise levels were visible in the narrowband case shown in Fig. 16, which explains the reduced power efficiency. For the wideband case in Fig. 17, the signal masked these so the difference between simulations is negligible.

In the closed-loop and the reference channel in the wireless test, the unwanted signals came from signal leakage and intermodulation products in the hardware. Therefore, a radar receiver bandwidth matched to the signal of interest and some efforts on resolving those would result in the expected values from simulations in the narrowband case. Therefore, it can be concluded that the measurement results are coherent with expected values.

C. MAXIMUM DETECTION RANGE

The experimental results for the relative error in maximum detection range are shown in Table 8.

It shows for the closed-loop test a good agreement with simulations with a relative error on multitones compared to chirp ranging from -2 to 16%. In the wireless test, overall chirp would have about 8-10% more range than multitones for narrowband (1 and 10 MHz). For ultra-wideband signals (150 and 800 MHz), the relative error is 2-5%. These differences were caused by the greater amount of distortion due to non-linear processes in the experimental test-bench. Therefore, the performances are stable for 8 and 10 bits as predicted in simulations

This still allowed confirmation of the stability of PMEPR and power efficiency with bit resolutions of 8 to 10 bits. For the closed-loop test, the performances were coarsely matched to the simulation results obtained with aa simple model of quantization. Thus simulation for high performance digitizers need not necessarily model the jitter to gauge maximum detection range.

D. SIGNAL-TO-NOISE RATIO (SNR)

The SNR is shown to be relatively constant over the parametric measurements for both chirp and multitones as shown in Table 9.

The SNR in closed-loop is consistent with simulations due to the difference in PMEPR between the studied signals. However, the SNR power for multitones in operational conditions seems to be on par with chirp. In closed-loop, the noise that is measured is caused by the clock jitter and the SNR limitation as shown in Table 4 has been estimated between 54.5 dBFS – 56.4 dBFS. The results shown here for SNR are between 43 and 52 dB and max power to full scale ADC

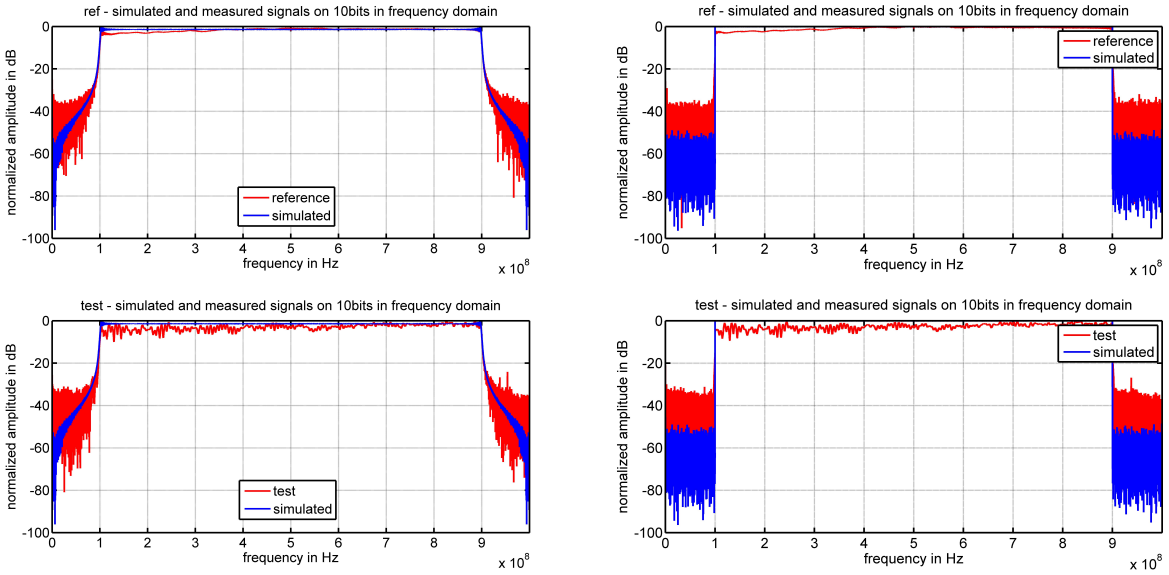

FIGURE 17. Measured spectra with 800 MHz bandwidth (left) chirp (right) multitones (top) reference channel (bottom) test channel a 10-bit resolution.

TABLE 8. Relative error in maximum detection range of multitones compared to chirp (%).

Bandwidth		1 MHz	10 MHz	150 MHz	800 MHz
CLL	ε(%)	[1.4; 16.3]	[1.4; 21.8]	[1; 13.4]	[-2.4; 16.3]
WT-RC	ε (%)	[-6.3; 10.9]	[0.6; 10.9]	[1.6; 4.4]	[-3.9; 2.2]
WT-TC	ε (%)	[5; 17.9]	[-3.4; 8.8]	[-4.35 1.9]	[-2; 5.5]

TABLE 9. SNR results on the parametric measurements in closed-loop and in operational conditions.

	Bandwidth	1 MHz	10 MHz	150 MHz	800 MHz
CLL	S+N (dBm)	[-8.9;-8.65]	[-8.9;-8.65]	[-8.6;-8.45]	[-8.7;-8.15]
	εS+N (dB)	[-2.65;-2.55]	[-2.7;-2.55]	[-2.6;-2.5]	[-2.6;-2.1]
	SNR (dB)	[43;47]	[45;52]	[46;52]	[45;52]
	εSNR (dB)	[-3;3.7]	[-4.5;5]	[-2.5;3.5]	[-3;3.7]
WT-RC	S+N (dBm)	[-6.5;-6]	[-6.1;-5.8]	[-6.2;-5.9]	[-7.4;-7.1]
	εS+N (dB)	[-0.22;0.02]	[0.02;0.2]	[-0.12;0.19]	[-0.28;0.1]
	SNR	[17.7;19.6]	[28.4;32.9]	[43.3;44.3]	[30.6;42.2]
	εSNR (dB)	[-3.5;-0.9]	[-2;-0.1]	[-0.8;4.7]	[-0.36;0.7]
WT-TC	S+N (dNm)	[-8.1;-7.8]	[-7.1;-6.9]	[-7.5;-7.1]	[-8.2;-7.8]
	εS+N (dB)	[-0.2;0.15]	[-0.03;0.14]	[-0.23;0.37]	[-0.36;0.18]
	SNR (dB)	[32.5;40.3]	[41.6;43.9]	[39.4;46.8]	[44;48.6]
	εSNR (dB)	[-2;1.1]	[-1.6;0.6]	[-0.35;0.75]	[-10.4;0.4]

range from 86% to 100%, meaning that the measurements are consistent with expectations taking into account distortions from hardware, thus confirming the validity of proposed equation (8).

The wireless test results came with somewhat of a surprise because the SNR was higher in the test channel than in the reference channel. Theoretically it should have been similar to the closed-loop results for the reference channel. Two hypotheses are assumed in contributing to this phenomenon. First, the frequency synthesizer used for the reference channel was not as stable as the one for the transmitter and since it is different the phase drift might have caused higher noise levels when demodulating the signal. The second is stronger intermodulation levels from the transmitting amplifier and demodulation stage in the reference channel since a filter is missing that would normally filter out-of-band contributors. They could have recombined, thus creating a semi-correlated base from which the noise is measured. As a general rule the SNR is stronger for the chirp than for multitones, however this distinction seems to fade as the wideband and stronger distortions characteristics appear.

E. SPURIOUS-FREE DYNAMIC RANGE (SFDR)

The SFDR including harmonics, one harmonic was recurring in every measurement be that chirp of multitones and it happened to be the strongest in most cases. As could be deducted instinctively, if a signal is present in all

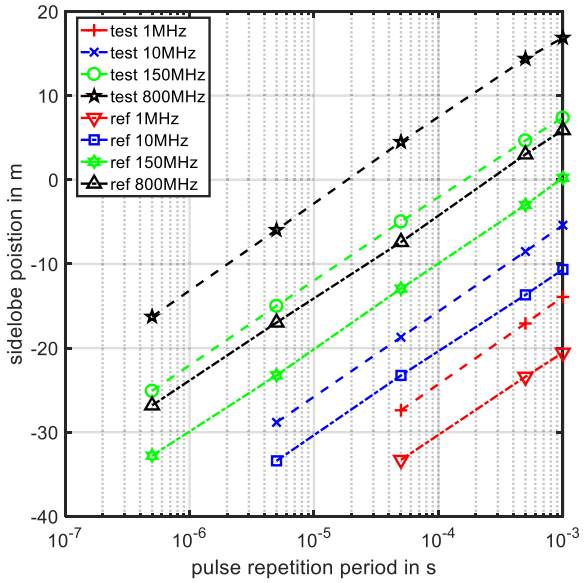

FIGURE 18. SFDR including harmonics (dBc) for multitones from the wireless test – maximum harmonic including DC for multitones.

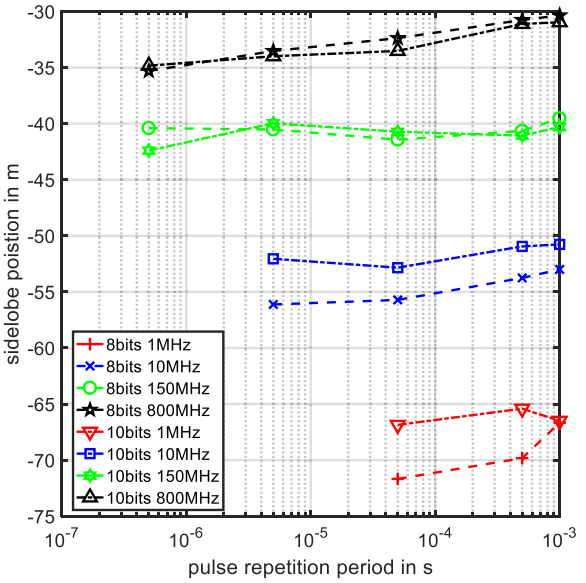

FIGURE 20. SFDR excluding harmonics (dBc) for multitones for the closed-loop test.

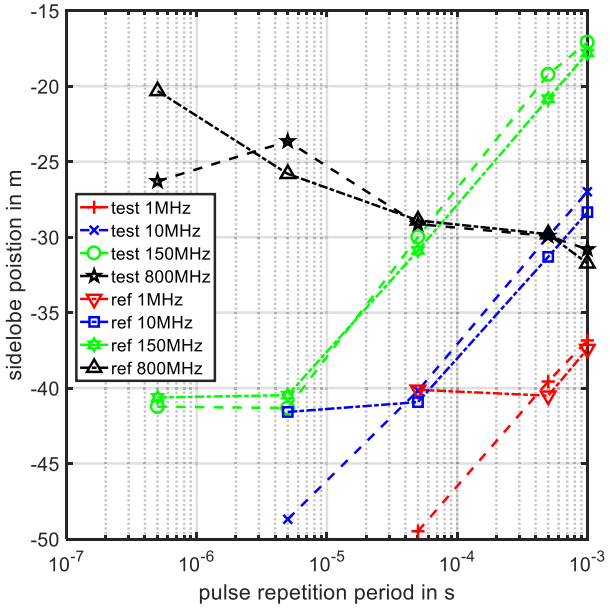

FIGURE 19. SFDR including harmonics (dBc) for multitones from the wireless test – maximum harmonic excluding DC for chirp.

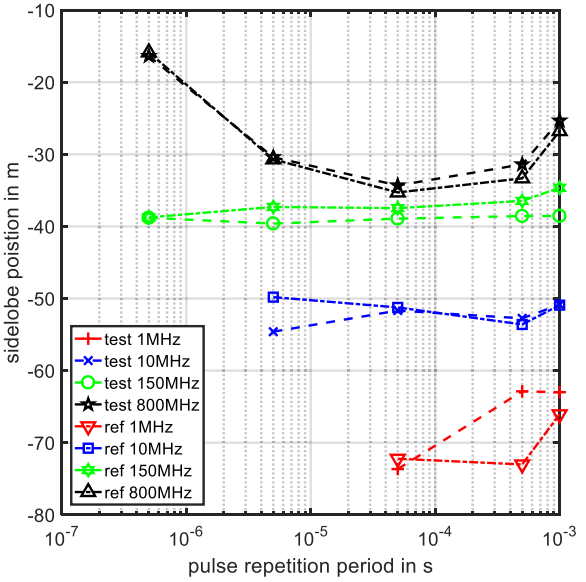

FIGURE 21. SFDR excluding harmonics (dBc) for multitones for the wireless test.

measurements regardless of the signal being recorded this means that its signal level will increase with pulse repetition period and with respect to the mean carrier level over the signal bandwidth of reference. From Fig. 18-19, a slope of 10dB per decade can be observed with respect to pulse repetition period and the signal level were also proportional to the bandwidth with some errors because of distortions but the main trends can be found from Fig.18-19 and Table 10.

The signal at DC was not eliminated even with bandpass filter so this is a combination of the DC harmonic resulting from a Hilbert transform and most likely leakage from the ADC clock or the local oscillator feeding the mixers for demodulation that would result in this particular harmonic. Other harmonics in the signal display such behaviors as shown in Fig. 19. In The signals with 800 MHz bandwidth were not as conclusive because it was harder to distinguish the harmonics from the random components visually.

This means that SFDR including harmonics could be dependent on *BT* product as it can be observed from Fig.18 for BT = 50 and 500, the corresponding points at 1MHz (50us,500us) and 10MHz(5us,50us) have similar levels.

The SFDR excluding harmonics (dBc) display relatively stable levels at a given bandwidth across the studied pulse

TABLE 10. SFDR including harmonics results on the parametric measurements in closed-loop and in operational conditions.

	Bandwidth	1 MHz	10 MHz	150 MHz	800 MHz
CLL	SFDR (dBc) – 50us PRP*	-34.6	-24.3	-13.5	-6.3
	εSFDR (dB)	[3.5;4.5]	[3.3;4.8]	[2.6;4.9]	[3.9;5.3]
	εBW_MT (dB)	N/A	[10.2;10.5]	[10.3;11]	[6.5;8]
	εBW_UpC (dB)	N/A	[9.7;10.3]	[11.3;12.2]	[5.1;5.8]
WT-RC	SFDR (dBc) – 50us PRP*	-26.3	-18.3	-6	4.5
	εSFDR (dB)	[0;0.25]	[0.2;0.8]	[0;1]	[0.1;0.8]
	εBW_MT (dB)	N/A	[8;8.9]	[12.3;12.8]	[9.6;10.7]
	εBW_UpC (dB)	N/A	[8.5;8.7]	[12.7;13.8]	[9;9.9]
WT-TC	SFDR (dBc) – 50us PRP*	-33.2	-23	-12.4	-7.1
	εSFDR (dB)	[0.2;1]	[0.22;0.5]	[0.16;1.1]	[0.1;0.9]
	εBW_MT (dB)	N/A	[10.1;10.4]	[10.2;11.1]	[5.3;5.8]
	εBW_UpC (dB)	N/A	[9.7;10]	[9.9;10.9]	[5.5;8.6]

* SFDR dBc increases 10dB per decade with pulse repetition period

TABLE 11. Highest PSLR in impulse response with Hamming window.

	Bandwidth	1 MHz	10 MHz	150 MHz	800 MHz
CLL	SFDR (dBc)	[-65.2;-60.9]	[-52.2;-48.6]	[-40.2;-38.1]	[-34.2;-29.5]
	εSFDR (dB)	[-1.5;2.4]	[0.4;4.2]	[-0.6;1.8]	[-7.8;0.6]
	εBW_MT (dB)	N/A	[10.4;15.8]	[9.8;14]	[5.7;9.5]
	εBW_UpC (dB)	N/A	[10.2;12.3]	[11.3;16.6]	[8;16]
WT-RC	SFDR (dBc)	[-63.7;-59]	[-52.6;-46.7]	[-39.4;-35]	[-31.5;-15.8]
	εSFDR (dB)	[0.6;1.4]	[0.3;6.3]	[0.9;2.2]	[3.1;3.3]
	εBW_MT (dB)	N/A	[6.4;15]	[11.5;17.5]	[4.1;7.3]
	εBW_UpC (dB)	N/A	[11.9;15.4]	[7.7;12.3]	[6.2;14.7]
WT-TC	SFDR (dBc)	[-55.7;-54.3]	[-48.1;-42.3]	[-36.3;-30.8]	[-26.9;-16.7]
	εSFDR (dB)	[0;2.8]	[0.3;2.9]	[0.3;3.2]	[0;5]
	εBW_MT (dB)	N/A	[9.7;12]	[8.4;13]	[6.5;9.6]
	εBW_UpC (dB)	N/A	[10.4;11.8]	[8;13.2]	[7.6;12.2]

repetition periods and seem to be directly proportional with the signal bandwidth as shown in Fig. 20-21 and quantified in Table 11. The results were also very similar between the closed-loop and the wireless tests. This indicates that the SFDR level could be independent of the pulse repetition period, SNR and that the spurs are a product of the signal frequency content and the distortions introduced by the ADC hardware. So this means that the SFDR levels excluding harmonics could only be dependent on bandwidth not time.

F. PULSE COMPRESSION

The pulse compression was performed with a digital replica for the closed-loop and both the reference signal and a digital replica for the wireless test. For wideband signals in Fig. 22, the right hand side of the pulse compression presents reflections when a Hamming window was applied. The higher the bandwidth was, the more visible the circuit imperfections. Indeed, problems with standing wave ratios in the experimental setup caused higher sidelobe levels at 150 and 800 MHz, Table 12 shows the highest peak-to-sidelobe ratio (PSLR) per bandwidth. The values for 1 and 10 MHz are nominal but it deteriorates for 150 and 800 MHz. Errors for 3 dB mainlobe width and sidelobes positions at 800 MHz, were caused by sample speck, perturbations induced by standing wave ratios in the circuit and for the test channel by multiple reflections from the environment. The proximity of the reflections from the main lobe associated with the sample speck error at 800 MHz in the wireless test may explain the degradation in sidelobe levels. To confirm this, an interpolation of the data was performed using 'interp' in Matlab by oversampling by 2 and lowpass filtering, the PSLR reached a maximum of 32 dB at 800 MHz bandwidth.

TABLE 12. Highest PSLR in impulse response with Hamming window.

Bandwidth	1 MHz	10 MHz	150 MHz	800 MHz
CLL	42.5 dB	42.5 dB	33.5 dB	37.2 dB
WT replica-ref	42.5 dB	42 dB	36.5 dB	28.1 dB (32dB with interp)
WT test-ref	41.5 dB	30 dB	24.5 dB	21.8 dB
WT test-replica	42.5 dB	30 dB	24.5 dB	25 dB

The pulse compression in wideband operation had PSLR under 30dB caused by standing wave ratios. The main limiting factor in wideband operation on contrast are the multiple reflections caused by standing waves as those ''ghost'' sidelobes can potentially mask smaller targets close to a bigger one. Alternatively deconvolution techniques such as CLEAN algorithms which have been modified for radar purposes e.g. [52], [53] could be used to compensate for the hardware impairments.

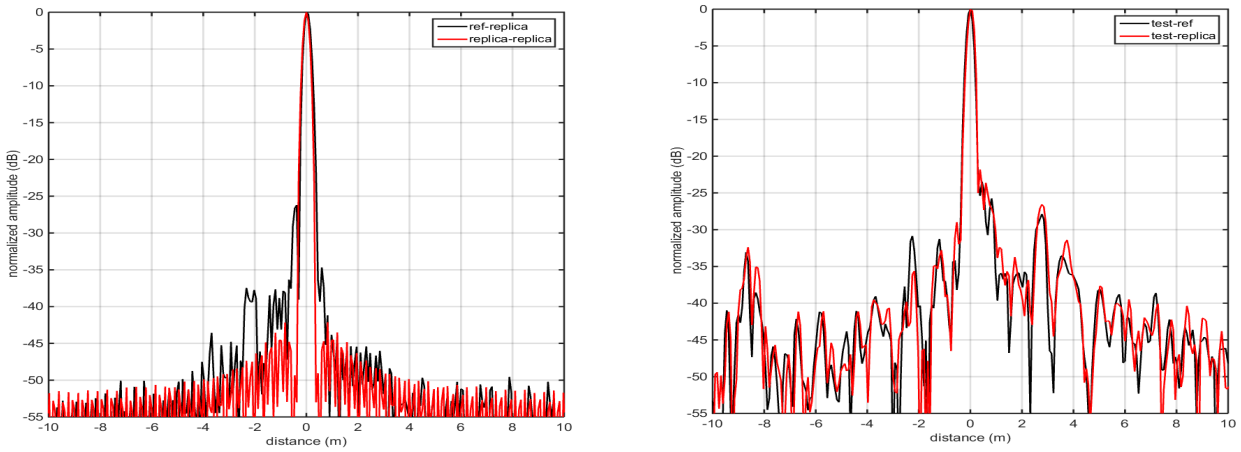

FIGURE 22. Compression in distance of multitones with BW = 800 MHz and PRP = 500ns with Hamming window – left) ref-replica and replica replica impulse responses- right) test-ref and test-replica impulse responses.

TABLE 13. Summary of simulation, experimental results and quantization + RF effects on radar performance.

		Simulation		Measurements	
		Results	Conclusions	Results	Conclusions
PMEPR		MT [3.01; 3.54] dB UpC [5.03; 5.63] dB	Bit resolution is not limiting at 10bits, UpC range is 10 to 16% greater than MT	Difference within 1.2 to 2.6dB in CLL ±1dB in full setup	Bit resolution is not limiting UpC range is 7 to 16% greater than MT in CLL; vary from -5.5 to 6% compared to MT in full setup
Pe		$Pe_{MT} > Pe_{UpC}$; $\varepsilon < 4$ %	res <6bits, reduced efficiency; res > 6bits, $\varepsilon_{Pe} < 2$% (nominal value)	PeMT ≈ PeUpC . if Rx BW ≈ signal BW	Negligible impact from 8-10 bits as predicted in simulation
SFDR incl.H				Increase of 10dB/dec with T, and proportionally with BW ratio for a fixed T.	
SFDR excl.H				Increase $10\log_{10}$ with BW ratio independent of T, SNR but rather on signal frequency content and INL, DNL introduced by ADC	
SNR	CLL	SNR limitation 54.5 - 56.4 dBFS cause by jitter		[43;52] dB for $P_{Sig\ max}$ [86;100]% of ADC $P_{in\ max}$	Limiting effect is jitter and not ENOB.
	RC			Inconsistent with CLL due to instability in synthesizer and recombination of intermodulation products in the bandwidth resulting in correlated noise levels	
	TC	Based on P_{ADCin_max} and theoretical Rx BW, NF, Gain of full setup test channel: $SNR_{max} \approx 43$dB		Generally, $SNR_{UpC} > SNR_{MT}$; however this distinction seems to fade as the wideband and stronger distortions characteristics appear.	
Compression	Main lobe	Identical performances	Temporal effect: Sample speck in distance (resolution, sidelobe positions) Amplitude quantization: negligible	Identical performances. PSLR <-32dB in CLL. SWR in wideband affects contrast. Partial compensation has potential; needs further tests to confirm.	Limiter on distance accuracy: sampling frequency but can be recovered with DSP, SWR effects compensated by cancelling the HW TF or the use of CLEAN algorithms.
	PSLR				
	Pedestal	Operationally, MT requires 2 more bit to match Chirp.			
Maximum detection range		Stable from 6bits R_{max_UpC} is 10 % to 15 % greater than R_{max_MT}; 10% if Rx BW ≈ signal BW		R_{max_UpC} is 8 % to 10 % greater than R_{max_MT}; Further range degradations are to be expected for typical MT codes with PMEPR up to 10-15dB; R_{max_UpC} is 50 % to 100 % greater than R_{max_MT};	

V. CONCLUSION

The performances of multitones and chirp for radar applications were investigated through simulations and experiments. This was done using waveform-independent criteria and a software-defined platform with hardware in the loop which supports any of the proposed waveform configurations without any modifications for an unbiased study with particular care given to the signal processing algorithm that is conservative in processing power, would be feasible with state-of-the-art FPGA chipsets and would relax constraints on reconfigurations and signal agility.

The experiments proved that the measurements matched coarsely the simulation results. This indicates that the experimental platform distorted signals further than anticipated but the small difference in performances between 8 to 10 bits was under 1 %, thus validating the required bit resolution for nominal performances for PMEPR and power efficiency.

A summary of the quantified results for chirp and P3 phase-coded multitones is given in Table 13 for simulations and experiments as well as the conclusions drawn from the results.

Operationally, a radar receiver bandwidth would closely match the signal bandwidth – for chirp typically 10% margin which multitones could potentially leverage this for higher spatial resolution or tighten the filter for increased SNR.

TABLE 14. Bandwidth-Time product configurations tested in simulation and experimentally for both chirp and multitones.

Pulse Repetition Period (µs)➔ / Bandwidth (MHz)➘	0.5	5	50	500	1000
1			17 dB	27 dB	30 dB
10		17 dB	27 dB	37 dB	40 dB
150	18.75 dB	28.75 dB	38.75 dB	48.75 dB	51.75 dB
800	26 dB	36 dB	46 dB	56 dB	59 dB

TABLE 15. Spatial resolution, fractional bandwidth and narrow band/ultrawide band classification based on Federal Communications Commission. FCC 02-48. 2002.

Bandwidth	1 MHz	10 MHz	150 MHz	800 MHz
Spatial resolution	150 m	15 m	1 m	0.1875 m
Fractional bandwidth in X band (RF stage)	0.0001	0.001	0.014	0.076
Classification in X band (RF stage)	NB	NB	NB	UWB (>500 MHz)
Fractional bandwidth in L band (IF stage)	0.00067	0.0067	0.1	0.533
Classification in L band (IF stage)	NB	NB	NB/UWB	UWB

TABLE 16. Waveform range and Doppler ambiguities based on the pulse repetition period.

Pulse Repetition Period (µs)	0.5	5	50	500	1000
Range ambiguity (m)	75	750	7500	75k	150k
Doppler ambiguity (Hz)	2M	200k	20k	2k	1k

The maximum detection difference between chirp and P3 phase-coded multitones in this case would be about 10%.

However, different phase codes overlaid on multitones would yield different performances, a higher PMEPR – like in communications from 10 dB typically up to 15 dB - would translate in a further reduction of maximum detection range – from 50 to 100% - compared to chirp as shown in Table 13.

Also the maximum achievable SNR using the full ADC dynamic range would be about 1 dB higher for chirp than for multitones, thus improving a little detection performances and consumption at the ADC. The proposed equation (8) was proven experimentally to predict SNR levels accurately.

The SFDR including and excluding harmonics showed signs of a dependency on *BT* product and bandwidth respectively. This could hint towards a way to predict SFDR levels from fewer measurements. However, further experiments are required to prove this particular point using different ADCs to confirm this is a rule and not just an isolated case.

Nowadays, converters e.g. AWG7122C [46], Proteus V6 [36], Calypso V6 [36], have improved sampling frequencies and most likely display better performances compared to that but it will increase the figure of merit of ADCs as described in [33]. Given that the mainstream ADCs will follow trends as described in [33], selecting appropriate ADCs for radar design is going to be even more critical. The required bit resolution for radar systems are mainly going to be driven by the requirements on contrast from the pulse compression using the predictive formula (10) and (12) but this has to be coupled with an appropriate clock source with a jitter level that would allow for the desired SNR as shown by (8) and not limited by ENOB when using complex waveforms. The empirical formula on contrast could be used but still needs to be validated experimentally. Although, it should be noted that different phase codes for multitones will yield different results, and simple simulations were sufficient to roughly predict expected performances.

The outcome of this study using a novel approach is that multitones are close in performances to chirp when the receiver bandwidth is equal to the signal bandwidth for phase codes that match P3PC performances in PMEPR.

Multitones opens to more flexibility in terms of signal diversity and spectrum reuse. The path towards multifunction, spectrum insertion, sub band independence and signal diversity is a complex question and the fusion of communication and radar front-ends are still an open problem and optimization problems for the optimization of radar and communications concurrently in different scenarios will emerge. The development of 5G technology and it's asynchronous and non-orthogonal waveforms could prove to be a valuable trend to follow to improve on radar waveform design and spectrum insertion.

APPENDIX

The radar data that was used is described further in Table 14 to 16, and was encoded in signed integers from 4 to 24 bits in increments of 2 in simulations and was measured with 8 and 10 bits experimentally.

REFERENCES

[1] G. Wunder *et al.*, "5GNOW: Non-orthogonal, asynchronous waveforms for future mobile applications," *IEEE Commun. Mag.*, vol. 52, no. 2, pp. 97–105, Feb. 2014.

[2] G. R. Al-Juboori, A. Doufexi, and A. R. Nix, "System level 5G evaluation of GFDM waveforms in an LTE-A platform," in *Proc. Int. Symp. Wireless Commun. Syst. (ISWCS)*, 2016, pp. 335–340.

[3] F. Schaich and T. Wild, "Waveform contenders for 5G—OFDM vs. FBMC vs. UFMC," in *Proc. 6th Int. Symp. Commun., Control Signal Process. (ISCCSP)*, 2014, pp. 457–460.

[4] L. Sit, C. Sturm, L. Reichardt, T. Zwick, and W. Wiesbeck, "The OFDM joint radar-communication system: An overview," presented at the 3rd Int. Conf. Adv. Satellite Space Commun. (SPACOMM), Budapest, Hungary, 2011.

[5] C. Sturm and W. Wiesbeck, "Waveform design and signal processing aspects for fusion of wireless communications and radar sensing," *Proc. IEEE*, vol. 99, no. 7, pp. 1236–1259, Jul. 2011.

[6] C. Sturm, Y. L. Sit, M. Braun, and T. Zwick, "Spectrally interleaved multi-carrier signals for radar network applications and multi-input multi-output radar," *Radar, Sonar Navigat., IET*, vol. 7, no. 3, pp. 261–269, Mar. 2013.

[7] D. Garmatyuk and K. Kauffman, "Radar and data communication fusion with UWB-OFDM software-defined system," in *Proc. IEEE Int. Conf. Ultra-Wideband*, Sep. 2009, pp. 454–458.

[8] G. Fettweis, M. Krondorf, and S. Bittner, "GFDM—Generalized frequency division multiplexing," in *Proc. IEEE 69th Veh. Technol. Conf. (VTC Spring)*, Apr. 2009, pp. 1–4.

[9] G. Lellouch, A. K. Mishra, and M. Inggs, "Design of OFDM radar pulses using genetic algorithm based techniques," *IEEE Trans. Aerosp. Electron. Syst.*, vol. 52, no. 4, pp. 1953–1966, Aug. 2016.

[10] M. Bică and V. Koivunen, "Generalized multicarrier radar: Models and performance," *IEEE Trans. Signal Process.*, vol. 64, no. 17, pp. 4389–4402, Sep. 2016.

[11] N. Levanon and E. Mozeson, *Radar Signals*. New York, NY, USA: Wiley, 2004.

[12] N. N. S. S. R. K. Prasad, V. Shameem, U. B. Desai, and S. N. Merchant, "Improvement in target detection performance of pulse coded Doppler radar based on multicarrier modulation with fast Fourier transform (FFT)," *IEE Proc.-Radar, Sonar Navigat.*, vol. 151, no. 1, pp. 11–17, Feb. 2004.

[13] F. Tigrek, "A processing technique for OFDM-modulated wideband radar signals," Ph.D. dissertation, Dept. Telecommun., Delft Univ. Technol., Delft, The Netherlands, 2010.

[14] R. F. Tigrek, W. J. A. D. Heij, and P. V. Genderen, "Solving Doppler ambiguity by Doppler sensitive pulse compression using multi-carrier waveform," in *Proc. Eur. Radar Conf.*, 2008, pp. 72–75.

[15] R. F. Tigrek and P. van Genderen, "Compensation of range migration for cyclically repetitive Doppler-sensitive waveform (OFDM)," *IEEE Trans. Aerosp. Electron. Syst.*, vol. 46, no. 4, pp. 2118–2123, Oct. 2010.

[16] G. Lellouch, P. Tran, R. Pribic, and P. van Genderen, "OFDM waveforms for frequency agility and opportunities for Doppler processing in radar," in *Proc. IEEE Radar Conf.*, May 2008, pp. 1–6.

[17] D. Garmatyuk, J. Schuerger, and K. Kauffman, "Multifunctional software-defined radar sensor and data communication system," *IEEE Sensors J.*, vol. 11, no. 1, pp. 99–106, Jan. 2011.

[18] D. Garmatyuk and M. Brenneman, "Adaptive multicarrier OFDM SAR signal processing," *IEEE Trans. Geosci. Remote Sens.*, vol. 49, no. 10, pp. 3780–3790, Oct. 2011.

[19] D. Garmatyuk, "Cross-range SAR reconstruction with multicarrier OFDM signals," *IEEE Geosci. Remote Sens. Lett.*, vol. 9, no. 5, pp. 808–812, Sep. 2012.

[20] C. Pfeffer, R. Feger, M. Jahn, and A. Stelzer, "A 77-GHz software defined OFDM radar," in *Proc. 15th Int. Radar Symp. (IRS)*, Gdańsk, Poland, 2014, pp. 1–5.

[21] J. R. G. del Arroyo and J. A. Jackson, "WiMAX OFDM for passive SAR ground imaging," *IEEE Trans. Aerosp. Electron. Syst.*, vol. 49, no. 2, pp. 945–959, APR. 2013.

[22] R. Baque, P. Dreuillet, and B. Vaizan, "CURACAO SAR/GMTI compact radar cube concept," in *Proc. Int. Conf. Radar*, Adelaide, SA, USA, Sep. 2013, pp. 81–84.

[23] P. Brouard, L. Constancias, A. Brun, S. Attia, J. Peyret, and P. Dreuillet, "Hycam: A new S band surface radar testbed," in *Proc. IET Int. Radar Conf.*, Xi'an, China, 2013, pp. 1–4.

[24] Y. Paichard, "Microwave camera for multi-dimensional analysis of the RCS of time-varying targets," Ph.D. dissertation, Dept. Phys. Electron., Univ. Paris-Sud, Orsay, France, 2007.

[25] O. A. Krasnov, L. P. Ligthart, Z. Li, G. Babur, Z. Wang, and F. van der Zwan, "PARSAX: High-resolution Doppler-polarimetric FMCW radar with dual-orthogonal signals," in *Proc. 18th Int. Conf. Microw. Radar Wireless Commun. (MIKON)*, Vilnius, Lithuania, 2010, pp. 1–5.

[26] M. T. Frankford, N. Majurec, and J. T. Johnson, "Software-defined radar for MIMO and adaptive waveform applications," in *Proc. IEEE Radar Conf.*, Washington, DC, USA, May 2010, pp. 724–728.

[27] S. Baskar and E. Ertin, "A software defined radar platform for waveform adaptive MIMO radar research," in *Proc. IEEE Radar Conf. (RadarCon)*, May 2015, pp. 1590–1594.

[28] C. Sturm, T. Zwick, W. Wiesbeck, and M. Braun, "Performance verification of symbol-based OFDM radar processing," in *Proc. IEEE Radar Conf.*, May 2010, pp. 60–63.

[29] W. Wiesbeck, "The radar of the future," in *Proc. Eur. Radar Conf.*, Oct. 2013, pp. 137–140.

[30] J. H. Kim, M. Younis, A. Moreira, and W. Wiesbeck, "Spaceborne MIMO synthetic aperture radar for multimodal operation," *IEEE Trans. Geosci. Remote Sens.*, vol. 53, no. 5, pp. 2453–2466, May 2015.

[31] G. Krieger, "MIMO-SAR: Opportunities and pitfalls," *IEEE Trans. Geosci. Remote Sens.*, vol. 52, no. 5, pp. 2628–2645, May 2014.

[32] S. H. Han and J. H. Lee, "An overview of peak-to-average power ratio reduction techniques for multicarrier transmission," *IEEE Wireless Commun.*, vol. 12, no. 2, pp. 56–65, Apr. 2005.

[33] B. E. Jonsson, "A survey of A/D-converter performance evolution," in *Proc. 17th IEEE Int. Conf. Electron., Circuits Syst.*, Dec. 2010, pp. 766–769.

[34] L. Bin, T. W. Rondeau, J. H. Reed, and C. W. Bostian, "Analog-to-digital converters," *IEEE Signal Process. Mag.*, vol. 22, no. 6, pp. 69–77, Nov. 2005.

[35] R. H. Walden, "Analog-to-digital converter survey and analysis," *IEEE J. Sel. Areas Commun.*, vol. 17, no. 4, pp. 539–550, Apr. 1999.

[36] Tekmicro. (2017), accessed on Jan. 17, 2017. [Online]. Available: www.tekmicro.com

[37] *EV10AQ190A*, e2V, Chelmsford, U.K., 2013.

[38] *ADC12J4000 12-Bit 4 GSPS ADC With Integrated DDC*, Texas Instrum., Dallas, TX, USA, 2014.

[39] G. Fettweis, M. Lohning, D. Petrovic, M. Windisch, P. Zillmann, and W. Rave, "Dirty RF: A new paradigm," *Int. J. Wireless Inf. Netw.*, vol. 14, no. 2, pp. 133–148, 2007.

[40] Xilinx. (2017). [Online]. Available: www.xilinx.com

[41] Altera. (2017). [Online]. Available: www.altera.com

[42] J. L. Kernec, D. Gray, and O. Romain, "Empirical analysis of chirp and multitones performances with a UWB software defined radar: Range, distance and Doppler," in *Proc. 2014 3rd Asia-Pacific Conf. Antennas Propag.*, vol. 2014, pp. 1061–1064.

[43] J. L. Kernec and O. Romain, "Empirical performance analysis of linear frequency modulated pulse and multitones on UWB software defined radar prototype," in *Proc. IET Int. Radar Conf.*, 2013, pp. 1–6.

[44] J. L. Kernec and O. Romain, "Multitones' performance for ultra wideband software defined radar," in *Applications of Digital Signal Processing through Practical Approach*, S. Radhakrishnan, Ed. Rijeka, Croatia: InTech, 2015.

[45] J. Le Kernec, O. Romain, P. Garda, and J. Denoulet, "Empirical comparison of chirp and multitones on experimental UWB software defined radar prototype," in *Proc. Conf. Design Archit. Signal Image Process.*, 2012, pp. 1–8.

[46] Tektronix. (2017), accessed on Jan. 17, 2017. [Online]. Available: www.tek.com

[47] R. G. Vaughan, N. L. Scott, and D. R. White, "The theory of bandpass sampling," *IEEE Trans. Signal Process.*, vol. 39, no. 9, pp. 1973–1984, Sep. 1991.

[48] S. Gifford, J. E. Kleider, and S. Chuprun, "OFDM transmitter power amplifier and PAR reduction performance: Measurement and simulation," in *Proc. MILCOM*, vol. 1. 2002, pp. 591–595.

[49] U. Kathree, W. Nel, V. J. van Rensburg, and A. K. Mishra, "Investigation of hopped frequency waveforms for range and velocity measurements of radar targets," in *Proc. IEEE Radar Conf.*, Oct. 2015, pp. 475–480.

[50] *IEEE Standard for Terminology and Test Methods for Analog-to-Digital Converters*, IEEE Standard 1241-2000, 2001.

[51] G. Fettweis, M. Lohning, D. Petrovic, M. Windisch, P. Zillmann, and W. Rave, "Dirty RF: A new paradigm," in *Proc. IEEE 16th Int. Symp. Pers., Indoor Mobile Radio Commun.*, vol. 4. Sep. 2005, pp. 2347–2355.

[52] R. Bose, "Lean CLEAN: Deconvolution algorithm for radar imaging of contiguous targets," *IEEE Trans. Aerosp. Electron. Syst.*, vol. 47, no. 3, pp. 2190–2199, Jul. 2011.

[53] H. Deng, "Effective CLEAN algorithms for performance-enhanced detection of binary coding radar signals," *IEEE Trans. Signal Process.*, vol. 52, no. 1, pp. 72–78, Jan. 2004.

JULIEN LE KERNEC (M'12) received the B.Eng. and M.Eng. degrees in electronic engineering from the Cork Institute of Technology, Ireland, respectively, in 2004 and 2006, respectively, and the Ph.D. degree in electronic engineering from University Pierre and Marie Curie, France, in 2011. He held a post-doctoral position with the Kuang-Chi Institute of Advanced Technology, Shenzhen, China, from 2011 to 2012. He was a Lecturer with the Department of Electrical and Electronic Engineering, The University of Nottingham Ningbo China, from 2012 to 2016. He is currently a Lecturer with the School of Engineering in the Systems, Power and Energy Group, University of Glasgow. His research interest includes radar system design, software defined radio/radar, signal processing, and health applications.

OLIVIER ROMAIN (M'11) received the B.Sc. degree in physics from University Louis Pasteur, France, in 1995, the M.Sc. degree in engineering from the Institut Télécom de Strasbourg in 1997, the M.Sc. degree in photonics and imaging from ULP, Strasbourg, France, and the Ph.D. degree in electronic engineering from University Pierre and Marie Curie, France, in 2001.

He was an Assistant Professor from 2002 to 2010 and then an Associate Professor from 2010 to 2011 with University Pierre and Marie Curie. Since 2011, he has been a Professor and the Head of the ASTRE Team, ETIS, University Cergy-Pontoise, France. His research interests include embedded systems for health and software-defined radio.